

High frequency intrinsic modes in El Niño/ Southern Oscillation Index

Filippo Petroni and Marcel Ausloos

GRAPES, B5, Sart-Tilman, B-4000 Liege, Belgium

Abstract

Recent *daily* data of the Southern Oscillation Index have been analyzed. The power spectrum indicates major intrinsic geophysical short periods. We find interesting “high frequency” oscillations at 24, 27, 37, 76, 100 and 365 days. In particular the 24 days peaks may correspond to the Branstator-Kushnir wave, the 27 days may be due to the moon effect rotation, the 37 days peaks is most probably related to the Madden and Julian Oscillation. It is not yet clear the explanations for the 76 days which may be associated with interseasonal oscillation in the tropical atmosphere; the 100 days could be resulting from a mere beat between the 37 and 27 periods, or the 76 and 365 days. Next these periods are used to reconstruct the signal and to produce a forecast for the next 9 months, at the time of writing. After cleansing the signal of those periodicities a detrended fluctuation analysis is performed to reveal the nature of the stochastic structures in the signal and whether specific correlation can be found. We study the evolution of the distribution of first return times, in particular between *extreme events*. A markedly significant difference from the expected distribution for uncorrelated events is found.

Key words:

1 Introduction

One of the most intriguing phenomena in climatology is known as *El Niño/Southern Oscillation* (ENSO), i.e. the more or less cyclic warming and cooling, mainly seen through an oscillation of about 6 – 8 years, of the eastern and central regions in the Pacific Ocean. El Niño is considered to be due to a disruption

Email address: Corresponding author fpetroni@gmail.com (Filippo Petroni).

of the ocean-atmospheric system in the tropical Pacific and is factually described by the so called *Southern Oscillation Index (SOI)* [1, 2, 3, 4], a proxy measure based on surface air pressure differences between Darwin, Australia and Tahiti, French Polynesia [5]. Data are usually analyzed from *monthly* averages.

Sustained negative values of the SOI often indicate El Niño episodes (see <http://www.bom.gov.au/climate/glossary/soi.shtml>). These negative values are usually accompanied by sustained warming of the central and eastern tropical Pacific Ocean, a decrease in the strength of the Pacific Trade Winds, and a reduction in rainfall over eastern and northern Australia. The most recent strong El Niño was in 1997/98. Positive values of the SOI are associated with stronger Pacific trade winds and warmer sea temperatures to the north of Australia, popularly known as a La Niña episode. Waters in the central and eastern tropical Pacific Ocean become cooler during this time. Together these give an increased probability that eastern and northern Australia will be wetter than normal. The most recent strong La Niña was in 1988/89; a moderate La Niña event occurred in 1998/99, which weakened back to neutral conditions before reforming for a shorter period in 1999/2000. This last event finished in Autumn 2000.

In our opinion wide window filtering and averaging techniques are nowadays unnecessary to obtain interesting informations. In fact, one of the most important problems in quantitative weather forecasting is to understand the nature (or structure) of stochastic processes which underline the weather evolution. One aspect of interest is to determine characteristics of the fluctuation distribution in a signal [6], leading to a probability distribution function (PDF) and their correlations. Empirical studies found that they are not (always) Gaussian distributed [7]. It was recently found e.g. for the southern oscillation index (SOI) [7] that long-range correlations may exist between the fluctuations of the index (even if it is still matter of debate [8]; moreover the PDF's have so called heavy tails ([9]), both features being describable through a Fokker-Planck equation approach. For such highly non linear systems higher frequency inputs of initial conditions in numerical simulations should be clearly helpful. Computer time would also be reduced if scaling laws are found or known, and propose criteria/constraints in iterating models.

Here below we report results of analysis of *daily* data downloaded from the Long Paddock - Climate Management Information for Rural Australia web site <http://www.longpaddock.qld.gov.au/SeasonalClimateOutlook/SouthernOscillationIndex/SOIDataFiles/index.html> for the time interval between Jan. 1999 and March 2007. We look for intrinsic mode periodicity and short/long term correlations present in the daily time series. We find interesting “high frequency” oscillations at 24, 27, 37, 76, 100 and 365 days. For correlation studies we use the detrended fluctuation analysis (DFA) method, equivalent to finding

the Hurst exponent [10, 11], on the *cleansed signal* (to be defined later).

Whence we reconstruct the signal, extrapolate for forecasting-like purpose for the next 9 months, at the time of writing. The presently objective observations seem to give some good agreement. We measure the so called area under the receiver operating curve as a test of forecasting quality [12, 13]. We get a 0.73 value for the area, a value which is usually considered quite good.

Moreover considering the signal as a random walk we can estimate the law of “first returns” for barrier level crossing, giving some quantitative information on the distribution time intervals even between *extreme events*. A markedly significant difference from the expected distribution for uncorrelated events is found. The dynamics of ENSO being sufficiently well represented in the daily data, we concur that a *daily* time series may be quite usefully employed for predicting events.

2 Data

Daily values of the *SOI* index for the time interval between Jan. 1999 and March. 2007 were downloaded from the Long Paddock - Climate Management Information for Rural Australia web site <http://www.longpaddock.qld.gov.au/SeasonalClimateOutlook/SouthernOscillationIndex/SOIDataFiles/index.html> for the longest period available at the time of finishing this study, (the web-site is updated daily). The raw data series is normalized through the standard deviation S of the sea level pressure (SLP) at a station in Tahiti and the sea level pressure at a station in Darwin.

$$SOI = \frac{P_{Tahiti} - P_{Darwin}}{S} \quad (1)$$

The data set consists of 3006 data points. The *SOI* daily data are plotted as a function of time in Fig. 1. The mean and standard deviation of this time series are respectively $\mu = -0.05$ and $\sigma = 1.57$.

It is sometimes stated that daily or weekly values of the SOI do not convey much in the way of useful information about the current state of the climate, and accordingly the Bureau of Meteorology does not issue them. Daily values in particular can fluctuate markedly because of daily weather patterns, and should not be used for climate purposes. We may disagree with this statement. There are indeed techniques which can sort out noise from coherent behavior and conversely. This shows the intent of using daily data.

3 Power spectrum

Instead of empirically searching for modes [14] we directly estimate the intrinsic fast (intra annual) modes from the power spectrum (PS) of the daily data following the algorithm proposed by [15]. The PS is estimated using the Multitaper Method (MTM) [16, 17] with $K = 5$ tapers. We chose this method because it is non parametric and reduces the variance of spectral estimates by using a small set of tapers [16, 17]. The PS obtained through MTM is shown in Fig. 2a on a linear-log plot. The PS of daily SOI is tested for significance relative to the null hypothesis of red noise (Fig. 2a) and locally white noise (Fig. 3a). A robust estimate of the red noise spectral background is found, following the work by [15], by minimizing the misfit between an analytical AR(1) (Auto Regressive process of order 1) red noise spectrum given by

$$S(f) = S_0 \frac{1 - r^2}{1 - 2r \cos(2\pi f / f_N) + r^2} \quad (2)$$

and the adaptively weighted multitaper spectrum which has been firstly convolved with a median smoother to reduce the weight of outliers in the least square fit. In equation (2) S_0 is the average value of the power spectrum, r is the lag-one autocorrelation and $f_N = 2/\Delta t$ is the Nyquist frequency ($\Delta t = 1$ day), the highest frequency that can be resolved with a sampling rate Δt . In the robust estimation S_0 and r are considered as free parameters for the minimization procedure. The PS is also tested against a locally white noise hypothesis (Fig. 3a).

The 95% and 99% confidence level (showed in the plots) for peaks detection are determined from the appropriate quantile of the χ -square distribution with $\nu = 2K$ degrees of freedom. From the plots we can say that the red noise background hypothesis is appropriate only for the first part of the spectrum (small frequency). In the frequency range $[0; 0.1]Hz$ both hypotheses on background noise give similar results on the number and positions of peaks exceeding the 99% confidence intervals. Quite different are instead the results for higher frequencies for which the spectrum of the SOI signal does not seem to be well fitted by a red noise spectrum.

From figures 2b and 3b one can recognize the position of several peaks at specific days (or for well defined periods) in the power spectrum. The positions of the highest peaks exceeding the 99% confidence interval are found to be roughly at 24, 27, 37, 76, 100 and 365 days; we did not consider those peaks which had small power even if exceeding the 99% confidence level, i.e. for frequencies greater than 0.1 cycles/days. Moreover we realize that each is an integer value, which is a first rough approximation with respect to the true geophysical period representing some event. Yet, some of these periodicities

may be related to well known geophysical processes [18]. In particular the 24 days peaks may correspond to the Branstator-Kushnir wave, a westward travelling wave with a period of about 23 days [19, 20, 21, 22, 23], the 27 days may be due to the moon effect rotation, the 37 days peaks is most probably related to the extratropical wave, so called Madden and Julian Oscillation (MJO) [24, 25]. It is not yet clear which explanations can be provided for the 76 days which may be associated with interseasonal oscillation in the tropical atmosphere, as discussed by [26] analyzing monthly SOI data; the 100 days could be resulting from a mere beat between the 37 and 27 periods, or the 76 and 365 days, which give respectively a 100 and a 96 day beating period, - or both jointly; the 365 days periodicity nature is obvious for those who regularly turn around the sun.

3.1 Signal reconstruction and forecasting

The results of the previous section can be used to reconstruct and forecast the future behavior of the daily SOI signal. We assume that the SOI signal can be modeled in time by the following stochastic process

$$SOI(t) = A_1(t) + \sum A_i(t) \cos\left(\frac{2\pi}{T_i}t + \phi_i\right) + \epsilon(t) \quad (3)$$

where $\epsilon(t)$ is a noise component, the nature of which should be determined, and T_i are the periods obtained in the previous analysis. The values for $A_i(t)$ and ϕ_i can be obtained from a time domain inversion of the spectral domain information contained in the K eigentapers [27, 28] but we prefer to model $A_i(t)$ as polynomial functions of degree n (in our case we consider $n = 1$, i.e. $A_i(t) = A_i + B_i t$) and to obtain the free parameters from a least square fitting procedure. In Fig. 4 we show the signal (dashed line) and the reconstructing function (solid line). The periods used for reconstruction are the following (the parameters A_i , B_i and ϕ_i obtained by the best fit procedure are summarized in Table 1): 70 months [9], 365 days, 100 days, 76 days, 37 days, 27 days and 24 days.

The function so obtained is then removed from the original SOI time series. A cleansed signal is obtained and the MTM spectrum is estimated again. In Fig. 5 we show a comparison of the power spectrum before and after removing the harmonic components from the daily SOI. One can recognize the portion of the spectrum due to the harmonic components. Both spectra are compared with the 95% and 99% confidence levels as described above for the red noise hypothesis. Recall that one relevant erroneous ingredient is the assumption of integer values for the considered geophysical periods. The error may accumulate for moderately short time series, but this assumption is hardly unavoidable.

In Fig. 6 we show the same reconstruction function from 01 Jan. 2006 and a possible forecast, based on this function, for the SOI for the next year (after March 2007 until 01 Jan. 2008). This function is shown together with a 95% confidence interval obtained through a cross validation procedure where each new data point is predicted using a model fitted only on the previous data points (so called “leave one out” validation).

In order to give another evaluation of the performance of our forecasting algorithm in predicting positive and negative SOI values we have also estimated the receiver operating curve (ROC) (plot in Fig. 7). The ROC [12, 13] is a widely used method to assess the validity of a binary classifier through the sensitivity and specificity as its discrimination threshold is varied. It is obtained as follows: in the first step SOI is digitalized based on the sign, the forecasted time series is similarly translated according to the signs (- and +). We then verify how good the forecast is by estimating the true positive and false positive rates (as shown in Figure 7), in the whole time window, varying the threshold used to discriminate between positive and negative values. The last step consists in estimating the area under the ROC, often called ROC AUC for which we obtained a value of 0.73.

4 Time correlations

Thereafter we can look for correlations in the cleansed signals, in which the main trends have been removed, through some estimator. This is important to understand the nature of the stochastic component in equation (3). Different estimators can be found in the literature for the long and/or short range dependence of fluctuations correlations [29, 30], one of the most precise and/or common is the detrended fluctuation analysis (DFA) method, see e.g. [31, 32, 33]. The method has been used previously to identify whether long range correlations exist in non-stationary signals, in many research fields such as e.g. finance [34, 35], cardiac dynamics [36] and of course meteorology [37, 38, 39], and by so many others that no exhaustive list can be here given. For an extensive list of references see [33]. Briefly, we recall that the signal time series $y(t)$ is *first integrated*, to ‘mimic’ a random walk $Y(t)$. The time axis (from 1 to N) is next divided into non-overlapping boxes of equal size n ; one looks thereafter for the best (polynomial, of degree m) trend, $z_{n,m}$, in each box, and calculates the root mean square deviation of the (integrated) signal with respect to $z_{n,m}$ in each box. The average of such values is taken at fixed box size n in order to obtain

$$F_m(n) = \sqrt{\frac{1}{N} \sum_{i=1}^N [Y(i) - z_{n,m}(i)]^2} \quad (4)$$

The box size is next varied over all possible n values and $F_m(n)$ recalculated. The resulting function is expected to behave like n^α indicating a scaling law. The value of α can be related to the fractal dimension and/or the Hurst exponent of the signal [11, 6].

In Fig. 8 we show a detrended fluctuation analysis of the cleansed daily SOI for linear ($m = 1$, DFA1) and quadratic ($m = 2$, DFA2) detrending. The resulting $F_m(n)$ functions can be usefully compared, from our point of view, with DFA1 of a synthetically generated Brownian motion with the same number of data points. It can be noticed looking at Fig 8 that $F_m(n)$ for the daily SOI, for both detrending, does not show a linear behavior for the whole range of n in the log-log plot, while the Brownian motion does. A not linear $F_m(n)$ function for the whole range of n may be due to the process not being long memory or to trends [33] still present in the cleansed data and which have not been removed from the algorithm used here, an open question therefore remains. Another method to assess long memory in stochastic processes is through the PS [41]. We then show the adaptively weighted multitaper spectrum ($S(f)$) of the cleansed series (Fig. 9) in a log-log plot. Also in this case a linear behavior, which would imply $S(f) \approx f^{-\beta}$, is not found in the whole frequency range indicating no simple self-affine behavior.

5 Return times

Another interesting point is the statistics of extreme (rare) events, namely those events that exceed a given threshold. Following previous studies we considered the cleansed SOI signal as the analog of a complex random walk and examine the distribution of first return times [42]. We studied the time interval r between two consecutive threshold crossing. The threshold q measures the strength of an event. The time series is firstly normalized such to have variance equal to 1, then a threshold $q = 1$ is chosen. We chose the same threshold for positive and negative “extreme” values. The results in Fig. 10 show the distributions for the time interval between consecutive positive, negative and both positive and negative threshold crossing. The return time interval distributions for cleansed SOI are compared with those of shuffled SOI. It is expected [43, 44] that while the latter should follow a Poisson distribution, as for uncorrelated events, long range correlated process should follow a stretched exponential distribution [43, 44]. The two kind of experimental distributions have been fitted with a Poisson distribution, for the shuffled SOI, and with a stretched exponential distribution, defined as

$$P(r) = \frac{a}{R} e^{-b(r/R)^\gamma} \tag{5}$$

for the cleansed SOI. In equation (5) R is the mean value of r , a , b and γ are free parameters. The exponent γ , for a long memory process x , is the same exponent that characterizes the autocorrelation function at lag s , $C_x(s) = \langle x_i x_{i+s} \rangle \approx s^{-\gamma}$. Figure 10 shows that while the shuffled data are well fitted by a Poisson distribution the cleansed SOI does not follow a Poisson distribution and it is closer to a stretched exponential one even if, due to the shortage of data, this result cannot yet be asserted with a good statistical significance test.

6 Conclusion

In contrast with many other works on SOI we have considered daily fluctuations instead of the more often used monthly averaged data. We have searched therefore for high frequency features, and observed intra annual major periods : 24, 27, 37, 76, 100 and 365 days. At periods shorter than 100 days, there is known evidence for very energetic westward propagating sea level signals at low latitudes (equatorward of about 20 deg latitude). The nature of this intraseasonal variability is usually thought to be distinctly different for periods longer and shorter than ca. 50 days. We have pointed out that each period is an integer value, which is a first rough approximation with respect to the true geophysical period representing some event. Yet, some of these periodicities may be related to well known geophysical processes. The 24 days may correspond to the Branstator-Kushnir wave, a westward travelling wave with a period of about 23 days [19, 20, 21, 22, 23], the 27 days may be tides due to the moon, the 37 days peaks is most probably related to the Madden - Julian Oscillation [24, 25]. It is not yet clear which explanations can be provided for the 76 days which may be associated with interseasonal oscillation in the tropical atmosphere [26]; the 100 days could be resulting from the beat between the 37 and 27 periods, or the 76 and 365 days, which give respectively a 100 and a 96 day beating period, - or both jointly.

These periods have been used, by modeling the SOI as a quasi-oscillatory signal plus “noise”, to reconstruct the time series and extrapolate it for forecasting purpose. The nature of the “noise” is also studied by removing from the SOI time series the reconstructed time series. Detrended fluctuation analysis together with power spectrum analysis have been employed in the attempt to understand the nature of the stochastic process showing that no simple scaling can be assessed. Through a systematic study of the distribution of first return times, we have indicated that extreme events cannot be considered uncorrelated.

This paper has not primarily aimed at writing up a model nor interpreting the intrinsic modes, on one hand, - this is found in already published work,

but rather in pointing out that daily, *quasi unaveraged* data can be used for medium range and high frequency forecasting.

Acknowledgements

Part of FP work has been supported by European Commission Project E2C2 FP6-2003-NEST-Path-012975 Extreme Events: Causes and Consequences. Critical and encouraging comments by B. Malamud, M. Ghil, P. Yiou, A. Witt and G. Rotundo have been very valuable for improving this report. Part of this work is related to activities in the COST P10 “Physics of Risk” program.

References

- [1] Vallis, G.K., (1988) Conceptual models of El Niño and the Southern Oscillation, *J. Geophys. Res.*, *93*, 13 979-13 991.
- [2] Philander S.G. (1999), El Niño and La Niña predictable climate fluctuations, *Rep. Prog. Phys.*, *62*, 123-142.
- [3] Ghil, M. and N. Jiang (1998), Recent forecast skill for the El Niño/Southern Oscillation , *Geophys. Res. Lett.* *25*, 171-174.
- [4] Keppenne C.L., and M. Ghil (1992), Adaptive spectral analysis and prediction of the Southern Oscillation Index, *J. Geophys. Res.*, *97*, 20449-20454.
- [5] Walker, G.T. , (1928) World Weather, *Q. J. R. Meteorol. Soc.* , *54*, 79-87.
- [6] Ausloos, M. (2002), Empirical Analysis of Time Series, in *From Quanta to Societies*, edited by W. Klonowski, pp 88-106, Pabst, Lengerich.
- [7] Ausloos, M. and K. Ivanova (2001), Power-law correlations in the southern-oscillation-index fluctuations characterizing El Niño, *Phys. Rev. E*, *63*, 047201-47204.
- [8] Metzler, R. (2003), Comment on “Power-law correlations in the southern-oscillation-index fluctuations characterizing El Niño”, *Phys. Rev. E*, *67*, 018201.
- [9] Ausloos, M. and F. Petroni (2007), Tsallis non-extensive statistical mechanics of El Niño Southern Oscillation Index, *Physica A*, *373*, 721-736.
- [10] Hurst, H.E. (1951), Long-term storage capacity of reservoirs *Trans. Amer. Soc. Civil Eng*, *116*, 770-808.
- [11] Turcotte, D. L. (1997) *Fractals and Chaos in Geology and Geophysics*, Cambridge Univ. Press, Cambridge.
- [12] Stanski, H.R., Wilson, L.J. and W.R. Burrows, (1989) Survey of common verification methods in meteorology *WMO/TD-N. 358*, *World Meteorological Organisation*, Geneva, Switzerland, 114 pp.
- [13] Stephenson, D.B., (2000) Use of the 'odds ratio' for diagnosing forecast skill, *Wea. and Forecas.*, *15*, 221-232.
- [14] Salisbury, J.I., and M. Wimbush (2002), Using modern time series analysis techniques to predict ENSO events from the SOI time series, *Nonlin. Proc. Geophys.*, *9*, 341-345.
- [15] Mann, M. E., and J. M. Lees (1996), Robust estimation of background noise and signal detection in climatic time series, *Clim. Change*, *33*, 409445.
- [16] Thomson, D. J., (1982) Spectrum estimation and harmonic analysis, *Proc. IEEE*, *70*, 10551096.
- [17] Percival, D. B., and A. T. Walden (1993), *Spectral Analysis for Physical Applications*, 583 pp., Cambridge Univ. Press, New York.
- [18] Kondrashov D., K. Ide, and M. Ghil (2004), Weather Regimes and Preferred Transition Paths in a Three-Level Quasigeostrophic Model, *J. Atmos. Sc.*, *61*, 568-587.

- [19] Branstator, G. W. (1987), A striking example of the atmosphere leading traveling pattern, *J. Atmos. Sci.*, *44*, 2310-2323.
- [20] Branstator, G. W. (1992), The maintenance of low-frequency atmospheric anomalies, *J. Atmos. Sci.*, *49*, 1924-1945.
- [21] Branstator, G. W. and I. M. Held (1995), Westward propagating normal modes in the presence of stationary background waves, *J. Atmos. Sci.*, *52*, 247-262.
- [22] Simmons, A. J., J. M. Wallace, and G. W. Branstator (1983), Barotropic wave propagation and instability and atmospheric teleconnection patterns, *J. Atmos. Sci.*, *40*, 1363-1392.
- [23] Kushnir, Y. (1987), Retrograding wintertime low-frequency disturbances over the North Pacific Ocean, *J. Atmos. Sci.*, *44*, 2727-2742.
- [24] Marcus, S.L., M. Ghil, and J.O. Dickey (1996), The Extratropical 40-Day Oscillation in the UCLA General-Circulation Model. 2. Spatial Structure, *J. Atmos. Sci.*, *53*, 1993-2014.
- [25] Ghil, M. and K. Mo (1991), Interseasonal oscillations in the global atmosphere. Part I: Northern Hemisphere and Tropics, *J. Atmos. Sci.*, *48*, 752-779.
- [26] Ghil, M., et al. (2002), Advanced spectral methods for climatic time series, *Rev. Geophys.*, *40*(1), 1003.
- [27] Park, J. (1992), Envelope estimation for quasi-periodic geophysical signals in noise: A multitaper approach, in *Statistics in the Environmental and Earth Sciences*, edited by A. T. Walden and P. Guttorp, pp. 189-219, Edward Arnold, London.
- [28] Mann, M. E., and J. Park (1994), Global scale modes of surface temperature variability on interannual to century timescales, *J. Geophys. Res.*, *99*, 25,819-25,933.
- [29] Taqqu, M.S., V. Teverovsky, and W. Willinger, (1995) Estimators for long-range dependence: an empirical study *Fractals*, *3*, 785-798.
- [30] Brockwell, P.J. and R.A. Davis (1991), *Time Series: Theory and Methods*, Springer-Verlag, Berlin,
- [31] Peng, C.-K., S. V. Buldyrev, S. Havlin, M. Simons, H. E. Stanley, and A. L. Goldberger (1994), Mosaic organization of DNA nucleotides, *Phys. Rev. E* *49*, 1685.
- [32] Bunde, A., S. Havlin, J. W. Kantelhardt, T. Penzel, J. Peter, and K. Voigt (2000), Correlated and Uncorrelated Regions in Heart-Rate Fluctuations during Sleep, *Phys. Rev. Lett.* *85*, 3736.
- [33] Hu, K., P.Ch. Ivanov, Z. Chen, P. Carpena and H.E. Stanley (2001), Effect of trends on detrended fluctuation analysis, *Phys. Rev. E*, *64*, 011114.
- [34] Vandewalle N., and M. Ausloos (1997), Coherent and random sequences in financial fluctuations, *Physica A*, *246*, 454-459.
- [35] Vandewalle N., and M. Ausloos (1998), Crossing of two mobile averages: an original method for measuring the roughness exponent, *Phys. Rev. E*, *58*, 6832-6834.

- [36] Ivanov, P. Ch., M. G. Rosenblum, C-K. Peng, J. Mietus, S. Havlin, H. E. Stanley, and A. L. Goldberger (1996), Scaling behaviour of heartbeat intervals obtained by wavelet-based time-series analysis, *Nature*, *383*, 323-327.
- [37] Ivanova, K., M. Ausloos, E. E. Clothiaux, and T. P. Ackerman (2000), Break-up of stratus cloud structure predicted from non-Brownian motion liquid water and brightness temperature fluctuations, *Europhys. Lett.* *52*, 40-46.
- [38] Ivanova, K. and M. Ausloos (1999), Application of the Detrended Fluctuation Analysis (DFA) method for describing cloud breaking, *Physica A*, *274*, 349-354.
- [39] Koscielny-Bunde, E., A. Bunde, S. Havlin¹, H. E. Roman, Y. Goldreich, and H.J. Schellnhuber (1998), Indication of a Universal Persistence Law Governing Atmospheric Variability, *Phys. Rev. Lett.* *81*, 729.
- [40] Pelletier, J.D., and D.L. Turcotte (1999), Self-affine time series: II. Applications and models, *Advances in Geophysics*, *40*, 91.
- [41] Malamud, B. D., and D. L. Turcotte (1999), Self-affine time series: I. Generation. and analyses. *Adv. Geophys.*, vol. 40, pp. 1-90.
- [42] Cimino G., G. Del Duce, L. K. Kadonaga, G. Rotundo, A. Sisani, G. Stabile, B. Tirozzi and M. Whitaric (1999), Time series analysis of geological data, *Chemical Geology*, *161*, 253-270.
- [43] Bunde, A., Jan F. Eichner, J. W. Kantelhardt, and S. Havlin (2005), Long-term memory: A natural mechanism for the clustering of extreme events and anomalous residual times in climate records, *Phys. Rev. Lett.*, *94*, 048701.
- [44] Eichner, F. Jan, J. W. Kantelhardt, A. Bunde, and S. Havlin (2006), Extreme value statistics in records with long-term persistence, *Phys. Rev. E*, *73*, 016130.

Table 1

Values of the parameter used for forecasting with a superposition of quasi-oscillatory signals.

| T | A | B | ϕ |
|-------------|--------|---------|--------|
| 70 months | -0.45 | 0 | 2.3 |
| 365 days | 0.58 | -0.0001 | 0.12 |
| 100 days | 0.004 | 0.0002 | 1.4 |
| 77 days | -0.028 | -0.0002 | 1.1 |
| 37 days | 0.38 | -0.0003 | 1.5 |
| 27 days | -0.084 | 0.0002 | 2.3 |
| 24 days | -0.008 | 0.0001 | 2.5 |
| linear term | 0.56 | -0.0005 | |

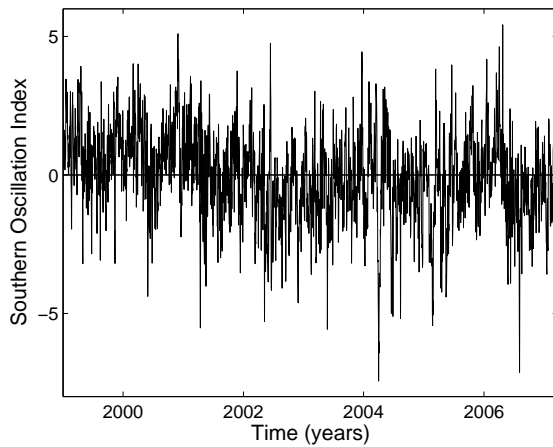


Fig. 1. Daily values of the Southern Oscillation Index (SOI) as defined in the text reported from 01 Jan. 1999 to 25 March 2007. Data are downloaded from <http://www.longpaddock.qld.gov.au/SeasonalClimateOutlook/SouthernOscillationIndex/SOIDataFiles/index.html>. Data series consists of 3006 data points.

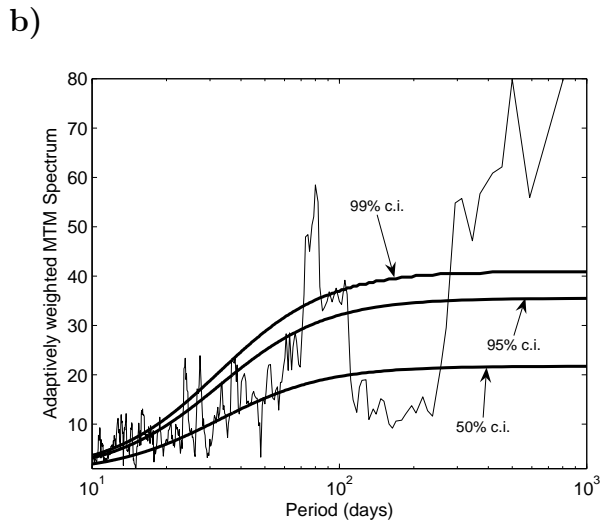
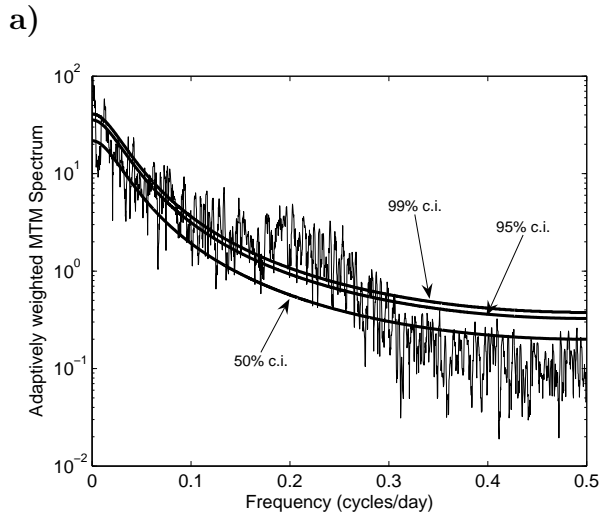
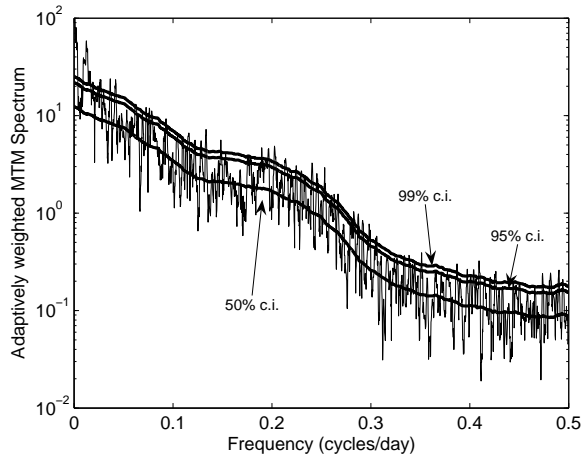


Fig. 2. a) Adaptively weighted multitaper power spectrum of SOI daily data as function of frequency. Continuous lines are red noise confidence interval. b) same as before but plotted as function of time (days) to highlight the periodicities in days of the SOI intrinsic high frequency modes. Continuous lines are red noise confidence interval.

a)



b)

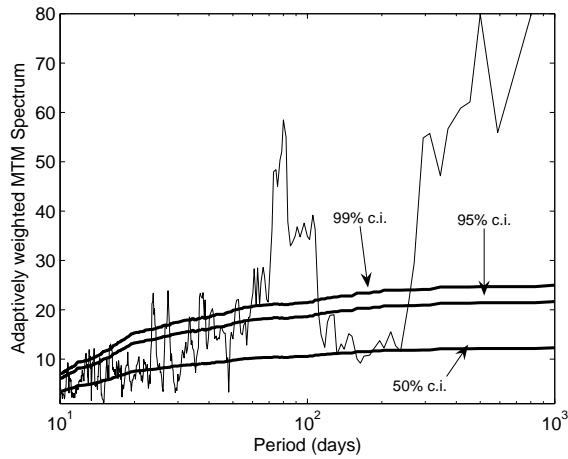


Fig. 3. a) Adaptively weighted multitaper power spectrum of SOI daily data as function of frequency. Continuous lines are locally white noise confidence interval. b) Same as before but plotted as function of time (days) to highlight the periodicities in days of the SOI intrinsic high frequency modes. Continuous lines are locally white noise confidence interval.

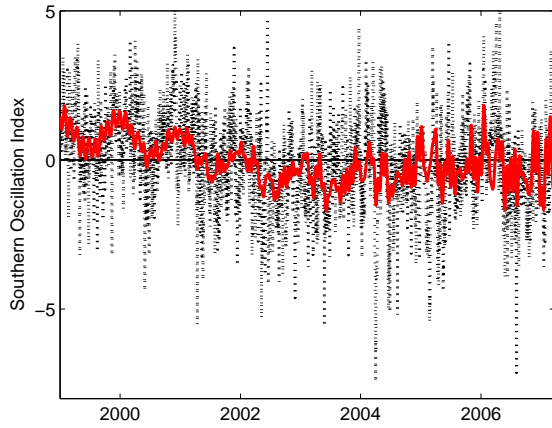


Fig. 4. Daily SOI signal and its reconstruction with basic periods as indicated in the text.

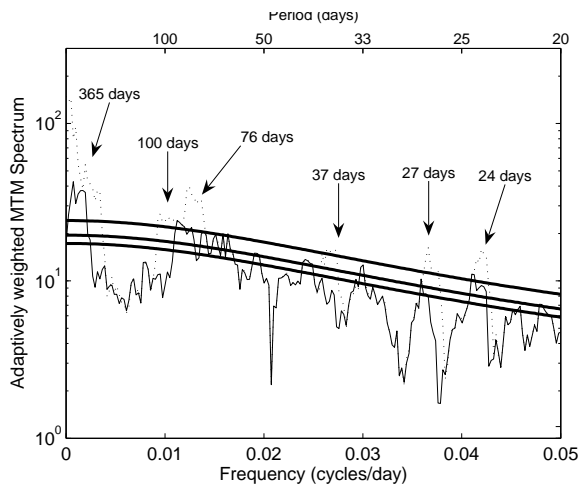


Fig. 5. Discrepancy between the adaptively weighted multitaper power spectrum of daily SOI (dashed line) and cleaned signal (solid line). The solid thicker lines represent the 90%, 95% and 99% confidence interval as explained in the text.

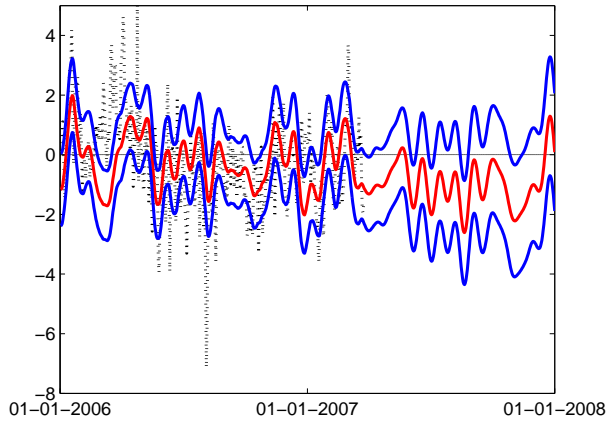


Fig. 6. Daily SOI (dashed line) together with the prediction (solid lines) based on the function described in the text. The upper solid and lower solid lines represent the 95% confidence interval estimated through a cross validation procedure (see text for details).

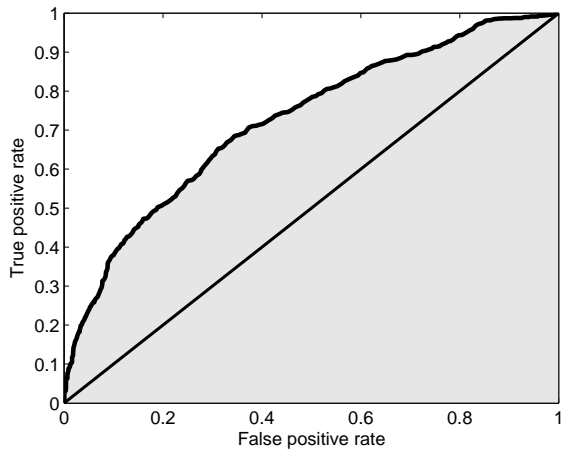


Fig. 7. Receiver operating curve (ROC), -thick line compared to random estimates, -straight line. The shadowed area represent the ROC AUC (see text)

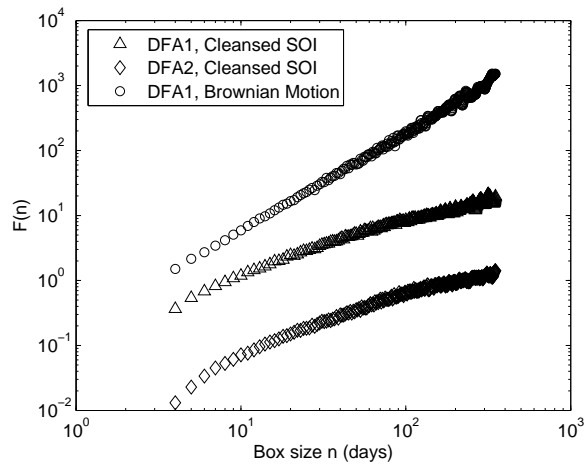


Fig. 8. DFA1 (triangles) and DFA2 (diamonds, amplitude divided by 10) of cleansed SOI compared with DFA1 (circles, amplitude multiplied by 10) of a Brownian motion with the same data points (3006). The slope α for Brownian motion is 1.5.

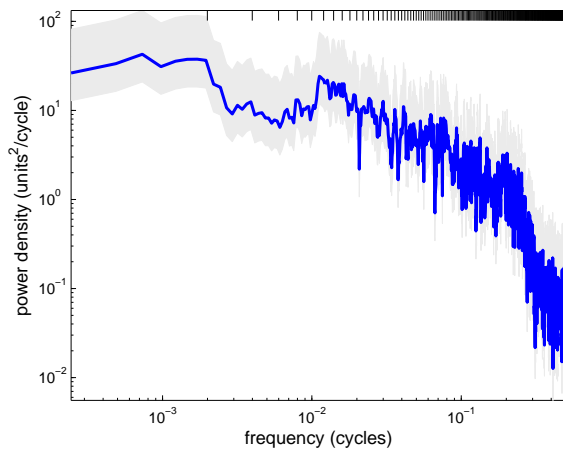


Fig. 9. Log-log plot of the adaptively weighted multitaper power spectrum of cleansed SOI daily data as function of frequency. Gray shadow indicates 95% confidence intervals.

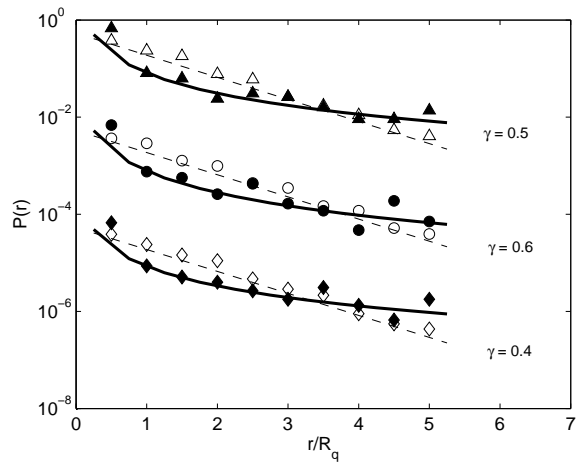


Fig. 10. Return interval distribution for events exceeding negative (diamonds), positive (circles) and both positive and negative (triangles) threshold with $q = 1$ for cleansed SOI data (filled symbols) and shuffled cleansed SOI data (open symbols). The two type of distributions are fitted respectively with a stretched exponential (solid line) and a Poisson distribution (dashed line). The values for γ are obtained through a least square fit.